published by Ural Federal University
eISSN 2411-1414
chimicatechnoacta.ru

ARTICLE
2024, vol. 11(3), No. 202411304
DOI:10.15826/chimtech.2024.11.3.04

Electrolytes in the $[N_{13}pip]ClO_4$-$LiClO_4$-Al_2O_3 system for solid state lithium batteries

Daria Kyzlasova [ab], Artem Ulihin [a *], Nikolai Uvarov [a]

a: Institute of Solid State Chemistry and Mechanochemistry SB RAS, Novosibirsk 630090, Russia
b: Novosibirsk State University, Novosibirsk 630090, Russia
* Corresponding Author: ulikhin@solid.nsc.ru

This paper belongs to a Regular Issue.

Abstract

The transport, electrochemical, structural, and thermal properties of electrolytes in the ternary system $[N_{13}pip]ClO_4$-$LiClO_4$-γ-Al_2O_3 ($N_{13}pip$ is N-methyl-N-ethyl-piperidinium cation) were investigated at the molar ratio $[N_{13}pip]ClO_4$:$LiClO_4$ = 0.82:0.18. The addition of alumina leads to a change in the thermodynamic properties of the $[N_{13}pip]ClO_4$-$LiClO_4$ system that can be explained by a partial transfer of lithium perchlorate from the organic phase to the surface of γ-Al_2O_3. The highest ionic conductivity of $6.2 \cdot 10^{-4}$ S/cm at 110 °C was observed for the composition containing the volume fraction (f) of γ-Al_2O_3 equal to 0.5. The increase in conductivity compared to the binary system $0.82[N_{13}pip]ClO_4$-$0.18LiClO_4$ is achieved due to the amorphization of the organic salt near the salt/$LiClO_4$/oxide interfaces. Galvanostatic cycling with Li electrodes shows that composites with f = 0.5 are stable at 110 °C for at least 68 charge/discharge cycles, and the electrolyte is shown to be electrochemically stable up to 5 V. This system can be used as a solid-state electrolyte in lithium-ion current sources.

Keywords

solid state ionics
organic ionic plastic crystals
lithium-ion current sources
solid composite electrolytes
ionic conductivity

Received: 11.06.24
Revised: 05.07.24
Accepted: 05.07.24
Available online: 19.07.24

Key findings

• The transport, electrochemical, structural, and thermal properties of electrolytes in the ternary system $[N_{13}pip]ClO_4$-$LiClO_4$-g-Al_2O_3 were investigated.

1. Introduction

Currently, lithium-ion current sources with liquid electrolytes are widespread. However, they have several disadvantages. Standard liquid electrolytes based on carbonates promote the lithium dendrite formation [1]. During the charge and discharge processes, non-uniform deposition of lithium occurs with the formation of needle-like structures – dendrites. Eventually, the dendrites can penetrate the separator and reach the cathode, causing a short circuit.

The second problem is related to the use of volatile solvents as a component of the liquid electrolyte. Due to the high saturated vapor pressure of these substances, there is a possibility of explosion and ignition of the device. In addition, due to mechanical instability, there is a risk of electrolyte leakage. Another problem of chemical power sources with liquid electrolytes is the need for a separator to prevent short circuits. All of the above problems can be solved by replacing liquid electrolytes with solid electrolytes.

Organic ionic plastic crystals (OIPCs) have been recently used as solid electrolytes [2, 3]. Plastic crystals have a solid-solid phase transition to the structurally disordered phases, which can promote ion transport [4, 5]. OIPCs have good electrochemical stability [6], low saturated vapor pressure, high thermal stability [7], small entropy of mixing [8], and a relatively high ionic conductivity [9], which is achieved due to the rotational movement of organic groups [10, 11]. OIPCs based on imidazolium

[12], pyrrolidinium [14], piperidinium, tetraalkylammonium [14], and tetraalkylphosphonium [15] are being actively studied. To use these substances as solid-state electrolytes, target metal cations must be incorporated into the OIPC matrix to enable ionic conductivity of the desirable type. For this reason, OIPCs may be doped with alkali metal salts [16–19]. Another way to increase the conductivity of solid electrolytes is the heterogeneous doping [20, 21]. Metal-organic frameworks, metal and non-metal oxides, polymeric nanoparticles and porous materials can be heterogeneous additives [22–25]. In this case, the ionic conductivity increases due to forming a defect-enriched region near the interface due to the surface interaction between the OIPC and the heterogeneous additive [26].

For example, the addition of aluminum oxide (γ-Al_2O_3) was shown to increase the values of specific conductivity of N-methyl-N-butylpiperidinium tetrafluoroborate by three orders of magnitude: from $2.04 \cdot 10^{-7}$ to $1.72 \cdot 10^{-4}$ S/cm at 100 °C [22]. Introducing a heterogeneous additive into organic OIPC-lithium salt systems can significantly affect their physicochemical properties. Ternary systems including OIPC, lithium salt, and polymeric nanoparticles were investigated [27,28]. It was found that the introduction of heterogeneous polyvinylidene fluoride (PVDF) in N-ethyl-N-methylpyrrolidinium tetrafluoroborate ($[C_2mpyr]BF_4$) doped with 10 mol% $LiBF_4$ increased the ionic conductivity in phase II from ~10^{-7} to ~10^{-5} cm/cm due to the formation of disordered phase located near the interfaces between OIPC and polymer nanoparticles. However, the conductivity of high-temperature phase I decreased from ~10^{-3} to ~10^{-5} S/cm.

N-methyl-N-propylpiperidinium perchlorate $[N_{13}pip]ClO_4$ is one of the salts belonging to the OIPC class. It is known from the literature that organic ionic salts with $[N_{13}pip]+$ cation and BF_4^-, PF_6^-, and Br^- anions are thermally stable up to nearly 230 °C. Still, their immobilization in such oxides as SiO_2 and MgO reduces the decomposition temperature [7]. It is also known that $[N_{13}pip]$TFSI salt (TFSI- is (trifluoromethylsulfonyl)imide cation) has a wide electrochemical stability window [29].

In the present work, the effect of heterogeneous additive Al_2O_3 on transport, thermal, structural, and electrochemical properties of the electrolytes in the $[N_{13}pip]ClO_4$-$LiClO_4$ binary system was studied. Lithium perchlorate has a high electrochemical stability when used in lithium batteries [30]. Preliminary studies showed that in the binary system, $[N_{13}pip]ClO_4$-$LiClO_4$ eutectics exists with the eutectics point at nearly 18 mol.% $LiClO_4$. At such a concentration of lithium salt, the system melts at 105 °C to a homogeneous liquid without the formation of other phases. That is why this composition was used for further investigations. The possibility of using the obtained composites as an electrolyte for lithium-ion batteries was investigated.

2. Experimental

2.1. Materials

N-methyl-N-propylpiperidinium perchlorate was synthesized in two steps. Firstly, 0.0827 mol of N-methyl piperidine, 0.1655 mol of n-propyl bromide, and 30 mL of acetonitrile were placed in a round bottom flask equipped with a magnetic stirrer and a reflux condenser. Then the mixture was boiled under stirring until the neutral reaction of wet indicator paper. As a result, N-methyl-N-propylpiperidinium bromide, $[N_{13}pip]Br$, was prepared according to the reaction:

$$CH_3NC_5H_{10} + CH_3CH_2CH_2Br \rightarrow [(CH_3)(CH_3CH_2CH_2)NC_5H_{10}]Br \quad (1)$$

The precipitate of $[N_{13}pip]Br$ was filtered off, washed with diethyl ether, and dried. In the second stage, a solution of 0.06736 mol $[N_{13}pip]Br$ in 20 mL water was added to 0.03368 M aqueous solution of lead perchlorate with the formation of a water solution of N-methyl-N-propylpiperidinium $[N_{13}pip]ClO_4$ by the reaction:

$$2[(CH_3)(CH_3CH_2CH_2)NC_5H_{10}]Br + Pb(ClO_4)_2 \rightarrow \rightarrow 2[(CH_3)(CH_3CH_2CH_2)NC_5H_{10}]ClO_4 + PbBr_2 \downarrow \quad (2)$$

The obtained solution was separated from $PbBr_2$ by filtration and evaporated. For removal of traces of lead chloride, the precipitate was dissolved in acetonitrile, the remaining precipitate was filtered, and then the solution was evaporated again. The obtained product was finally recrystallized from a mixture of ethyl acetate and ethyl alcohol.

Lithium perchlorate was synthesized by the reaction between perchloric acid $HClO_4$ and lithium carbonate Li_2CO_3 according to the reaction:

$$2HClO_4 + Li_2CO_3 \rightarrow 2LiClO_4 + H_2O + CO_2 \uparrow \quad (3)$$

Aluminum oxide γ-Al_2O_3 (surface area 200 m^2/g, specification IKT-02-6M; JSC Katalizator, Novosibirsk, Russia) was preheated in a muffle furnace at 600 °C for 2 h for dehydration.

To obtain the composites, $[N_{13}pip]ClO_4$ was mixed with $LiClO_4$ in a molar ratio of 0.82:0.18 with the addition of ethyl alcohol. The obtained mixture was dried in air and then in a vacuum oven at 170 °C for 12 h. The obtained binary system was mixed in with γ-Al_2O_3 in different ratios in the concentration range of 30–80 vol.% of γ-Al_2O_3. Further in the text, the parameter *f* will indicate the volume fraction of aluminum oxide.

2.2. Methods

The thermal properties of composites were investigated by differential scanning calorimetry using a DSC500 device. The samples were placed in aluminum pans and heated at a rate of 10 °C/min. The analysis was performed in an argon atmosphere at a flow rate of 0.05 L/min. The data recorded at the second heating are

 DOI:10.15826/chimtech.2024.11.3.04

presented in the paper. The structural properties were studied by X-ray diffraction on a BRUKER D8 ADVANCE diffractometer. For conductivity measurements, of the composites were compacted at 400 bar to pellets 0.5 cm in diameter with silver electrodes. The measurements were carried out at AC voltage in the frequency range of 30 Hz – 1 MHz by HP-4284A Hewlett Packard Precision LCR Meter in a vacuum of $5 \cdot 10^{-2}$ Torr in a stepwise temperature change mode in the range of 25–150 °C. Electrochemical studies were carried out on CR2032-type cells assembled in a glove box in an argon atmosphere. Electrochemical stability in contact with metallic lithium was investigated by galvanostatic cycling of symmetric cells with lithium electrodes at a current density of 0.05 mA/cm² and a temperature of 110°C. Impedance data were obtained after cycling using the Electrochemical station Zive SP2. The electrochemical window was determined by linear voltammetry using a SmartStat PS-50 instrument at T = 110 °C. Stainless steel was used as the working electrode, and lithium metal was used as the reference electrode. The rate of potential sweep was 1 mV/s.

3. Results and Discussion

3.1. Thermal properties

During the first heating of the initial three-phase mixture from 25 to 190 °C, the interaction between the components takes place, accompanied by several peaks due to phase transitions in the organic salt and dehydration of the components. Therefore, for further analysis, only data obtained during the second heating were used. Figure 1 shows the as-obtained DSC curves in the temperature range of 30–190 °C.

A pure organic salt $[N_{13}pip]ClO_4$ has two overlapping thermal effects at 117 °C and 125 °C. The first peak refers to the transition to the high-temperature disordered phase characteristic of this class of compounds, and the second peak refers to melting. Two thermal effects are also observed for $[N_{13}pip]ClO_4$ containing 0.18 mole fraction of lithium perchlorate at T ~60 °C and T ~105 °C. The first thermal effect is due to the polymorphic phase transition, while the second one is due to melting. The decrease in melting temperature is due to the formation of a eutectic mixture with the composition $0.82[N_{13}pip]ClO_4$-$0.18LiClO_4$. After doping with heterogeneous additive γ-Al_2O_3 in an amount of 30 vol.%, two thermal effects are observed at temperatures corresponding to the temperatures of thermal effects of pure organic salt. A possible reason for the observed effect is the high adhesion of lithium perchlorate to the surface of the oxide additive. As a result, the salt is practically completely transferred to the surface of the γ-Al_2O_3 particles, leading to the disintegration of the eutectic mixture to the mixture of pure $[N_{13}pip]ClO_4$ in which $LiClO_4/Al_2O_3$ particles are embedded. At higher concentrations of the γ-Al_2O_3, the intensity of the thermal effects of the ionic salt decreases, and at the volume fraction of γ-Al_2O_3 $f \geq 0.5$, the thermal effects due to phase transition and melting of the salt vanish. The most possible reason for this is the transition of the salt to the amorphous state. This effect is typical for ionic salt-oxide systems and was previously observed in the systems $LiClO_4$-A (A = MgO [31], Al_2O_3 [32]), $(n\text{-}Bu)_4NBF_4$-Al_2O_3 [33], $[(CH_3)(n\text{-}C_4H_9)NC_5H_{10}]BF_4$-X (X = SiO_2, Al_2O_3) [22], $(n\text{-}C_4H_9)NBF_4$-Y (Y=MgO, Al_2O_3) [34, 35], N-ethyl-N-methyl pyrrolidinium bis(trifluoromethane sulfonyl)amide (C_2mpyr[TFSI]) – Z (Z = TiO_2, SiO_2) [36]. It was also observed in OIPC-polymer composite systems by NMR [37, 38].

3.2. Structural properties

Figure 2 shows the data of X-ray phase analysis of both initial compounds ($[N_{13}pip]ClO_4$, $LiClO_4$, the binary system $0.82[N_{13}pip]ClO_4$-$0.18LiClO_4$ before and after doping with aluminum oxide.

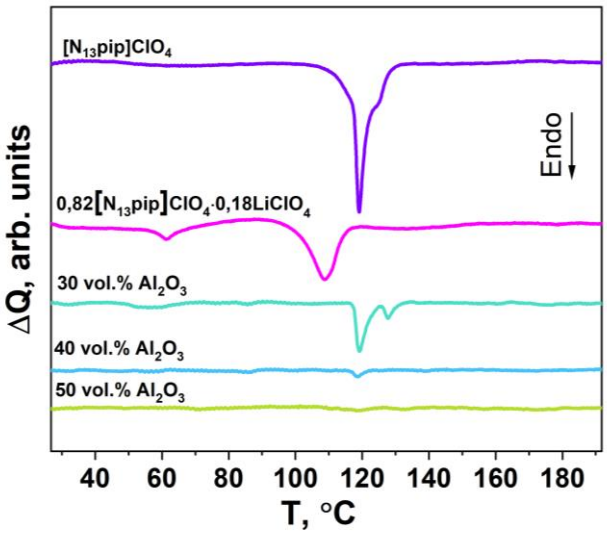

Figure 1 The DSC curves for some $[0.82N_{13}pip]ClO_4$-$0.18LiClO_4$-Al_2O_3 composites.

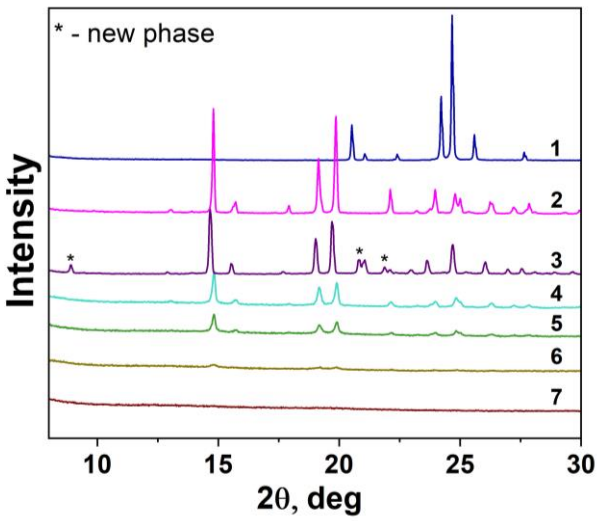

Figure 2 The diffraction patterns of pure $LiClO_4$ (1), pure $[N_{13}pip]ClO_4$ (2), initial mixture $0,82[N_{13}pip]ClO_4$-$0,18LiClO_4$ (3) and composites $0,82[N_{13}pip]ClO_4$-$0,18LiClO_4$-Al_2O_3 containing 30, 40, 50 and 60 vol.% alumina, curves (4), (5), (6) and (7), respectively.

 DOI:10.15826/chimtech.2024.11.3.04

It can be seen that in the binary system, there are reflections of pure N-methyl-N-propylpiperidinium perchlorate and reflections that do not correspond to any of the initial components of the mixture. These reflections may be related to a new phase of double salt. To identify a new phase, the phase diagram of the binary system $[N_{13}pip]ClO_4$-$LiClO_4$ should be investigated. Such work is in progress now. The introduction of γ-Al_2O_3 heterogeneous additive results in two effects (see curves (4)–(7) in Figure 2): (i) only the reflections corresponding to pure $[N_{13}pip]ClO_4$ are present in the X-ray patterns of $0.82[N_{13}pip]ClO_4$-$0.18LiClO_4$-Al_2O_3 composites. The observed effect correlates well with the results of differential scanning calorimetry and confirms the assumption that lithium perchlorate is adsorbed on the surface of aluminum oxide as an amorphous layer which gives no X-ray diffraction peaks; (ii) a marked decrease in the intensity of the reflections with increasing concentration of the heterogeneous dopant is observed. At the concentration of γ-Al_2O_3 ≥ 60 vol.%, these reflections completely disappear. This effect also correlates with the data of thermal analysis, which confirms the assumption of partial or complete amorphization of N-methyl-N-propylpiperidinium perchlorate in the composites.

3.3. Transport properties

The dependence of specific conductivity on temperature is presented in Figure 3 in Arrhenius coordinates. Conductivity parameters are listed in Table 1. The conductivity values are reproduced in heating-cooling cycles, which indicates that the conductivity is not associated with metastable defects and is not due to protons of water adsorbed on the composite surface. The values of specific conductivity of the electrolyte $0.82[N_{13}pip]ClO_4$-$0.18LiClO_4$ abruptly change due to melting from nearly 10^{-7} S/cm to 10^{-3} S/cm (Table 1).

The addition of the heterogeneous additive leads to an increase in conductivity at temperatures below the melting point. At low concentrations of $0.1 \le f \le 0.4$ as well as for the pure $0.82[N_{13}pip]ClO_4$-$0.18LiClO_4$ electrolyte, sharply increasing conductivity associated with melting is observed due to residual quantity of free salt or eutectics in the composites. At concentrations $0.5 \le f \le 0.8$, no jump change in conductivity is observed. Moreover, at a concentration of, $f = 0.5$, the temperature dependence of conductivity is not linear in Arrhenius coordinates. The observed effect may be related to the fact that at $f \le 0.5$ the conductivity curves can be described by Arrhenius dependences over the whole temperature region.

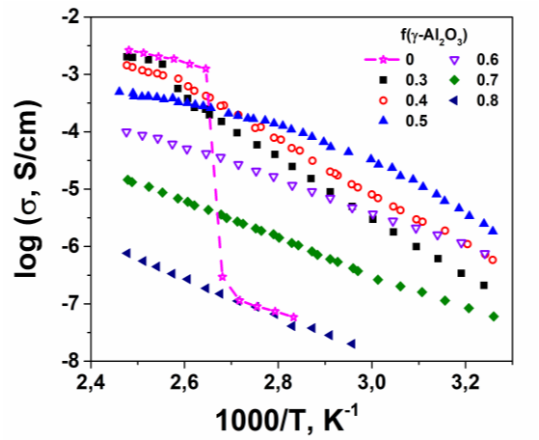

Figure 3 The temperature dependence of conductivity for composites (The third heating).

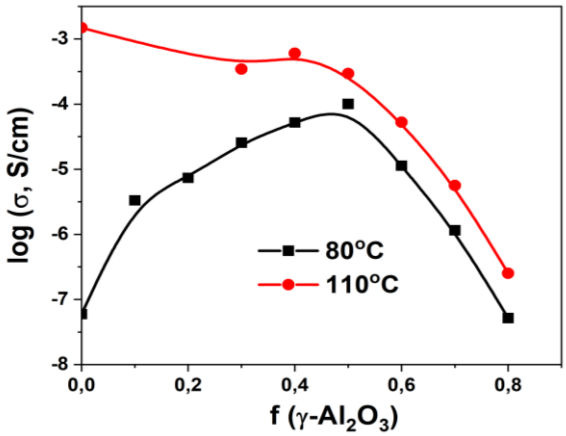

Figure 4 The dependence of composites conductivity on the volume fraction of Al_2O_3.

Table 1 Ionic conductivity parameters of $(1-f)\{0.18[N_{13}pip]ClO_4$-$0.82LiClO_4\}$-$fAl_2O_3$ composites, where f is the volume fraction of alumina.

f	σ_{80} (S/cm)	σ_{110} (S/cm)	E_a (eV)	log *A*
0	$5.8\cdot10^{-8}$	$1.5\cdot10^{-3}$	0.52±0.02[a] 0.35±0.02[b]	2.8±0.2[a] 4.4±0.3[b]
0.1	$8.3\cdot10^{-6}$	–	1.20±0.02	14.8±0.3
0.2	$7.4\cdot10^{-6}$	–	1.25±0.03	15.1±0.4
0.3	$2.5\cdot10^{-5}$	$3.8\cdot10^{-4}$	1.06±0.01	13.1±0.1
0.4	$5.2\cdot10^{-5}$	$6.2\cdot10^{-4}$	0.96±0.01	11.9±0.1
0.5	$1.1\cdot10^{-4}$	$3.2\cdot10^{-4}$	VFT [c]	VFT [c]
0.6	$1.2\cdot10^{-5}$	$5.0\cdot10^{-5}$	0.60±0.01	6.20±0.08
0.7	$1.2\cdot10^{-6}$	$6.0\cdot10^{-6}$	0.65±0.01	5.92±0.07
0.8	$4.1\cdot10^{-8}$	$2.7\cdot10^{-7}$	0.68±0.01	5.0±0.2

[A] below melting temperature;
[B] above melting temperature;
[C] curve is non-linear in Arrhenius coordinates and can be described by Vogel-Fulcher-Tamman (VFT) equation.

 DOI:10.15826/chimtech.2024.11.3.04

The thermal, structural, and conductivity data can be interpreted in terms of the qualitative scheme presented in Figure 5. The overall concentration range can be separated into four regions:

– at low concentration of the alumina below the first percolation threshold all oxide particles are covered with the $LiClO_4$ layer, which in turn is covered by a layer of the amorphous phase of $[N_{13}pip]ClO_4$ located near the $LiClO_4/[N_{13}pip]ClO_4$ interfaces. As lithium perchlorate partially transfers from the initial composite to the alumina surface, the remaining volume of the composite is depleted in $LiClO_4$;

– as the concentration of alumina rises, the volume fraction of the amorphous phase increases; at $f \sim 0.5$ this phase occupies a total volume of $[N_{13}pip]ClO_4$ in the composites, and the conductivity reaches a maximum. The conductivity of the amorphous phase has non-Arrhenius behavior and can be described by the Vogel-Fulcher-Tamman equation, which is typical of amorphous compounds [39–41];

– further increase in the oxide additive content leads to a decrease in the concentration of the amorphous phase of $[N_{13}pip]ClO_4$, and at sufficiently high concentration of oxide, in the vicinity of the second percolation threshold, ionic transport occurs along the $LiClO_4/Al_2O_3$ interfaces.

– the conductivity is due to $[N_{13}pip]ClO_4$, which is in the amorphous state. Interestingly, at $f > 0.5$, $s(T)$ dependences follow Arrhenius dependences over the whole temperature region.

The thermal, structural, and conductivity data can be interpreted in terms of the qualitative scheme presented in Figure 5. The overall concentration range can be separated into four regions:

– at low concentration of the alumina below the first percolation threshold all oxide particles are covered with the $LiClO_4$ layer, which in turn is covered by a layer of the amorphous phase of $[N_{13}pip]ClO_4$ located near the $LiClO_4/[N_{13}pip]ClO_4$ interfaces. As lithium perchlorate partially transfers from the initial composite to the alumina surface, the remaining volume of the composite is depleted in $LiClO_4$;

– as the concentration of alumina rises, the volume fraction of the amorphous phase increases; at $f \sim 0.5$ this phase occupies a total volume of $[N_{13}pip]ClO_4$ in the composites, and the conductivity reaches a maximum. The conductivity of the amorphous phase has non-Arrhenius behavior and can be described by the Vogel-Fulcher-Tamman equation, which is typical of amorphous compounds [39–41];

– further increase in the oxide additive content leads to a decrease in the concentration of the amorphous phase of $[N_{13}pip]ClO_4$, and at sufficiently high concentration of oxide, in the vicinity of the second percolation threshold, ionic transport occurs along the $LiClO_4/Al_2O_3$ interfaces. As shown earlier [32] nanocomposites $LiClO_4$-Al_2O_3 have a high ionic conductivity. Despite this, in the composites under study the concentration of $LiClO_4$ is not sufficiently high, the conductivity can be measured up to $f = 0.8$;

– at very high alumina concentrations above the second percolation threshold the conductive regions are separated, all conductivity pathways are broken, and the composites are insulators.

Table 2 shows the conductivity of some composite electrolytes found in the literature. It can be said that the transport properties of our system are comparable to those of other composite electrolytes.

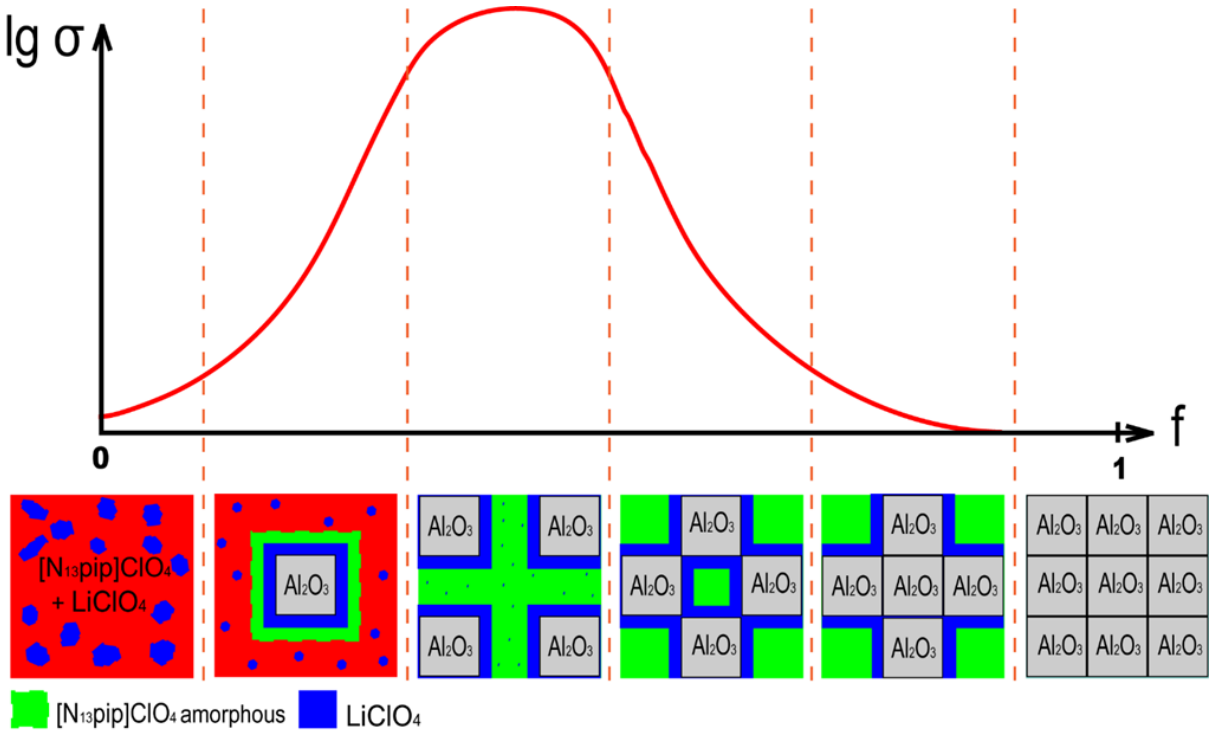

Figure 5 Schematic representation of composite morphology and conductivity isotherm as a function of oxide additive concentration.

 DOI:10.15826/chimtech.2024.11.3.04

Table 2 Conductivity of some composite electrolytes.

System	Conductivity at 40 °C	Reference
PEO-$LiClO_4$-Al_2O_3	~$2{\cdot}10^{-5}$	[42]
LLZTO/PVDF-HFP	~$3{\cdot}10^{-5}$	[43]
PAN-TiO_2-$LiClO_4$	~$6{\cdot}10^{-6}$	[44]
[C_2mpyr][TFSI]- LiTFSI-polymer nanoparticles	~$1{\cdot}10^{-7}$	[27]
$LiClO_4$-Al_2O_3	~$2{\cdot}10^{-5}$	[32]
[N_{13}pip]ClO_4-$LiClO_4$-Al_2O_3	~$4{\cdot}10^{-6}$	This work

3.4. Galvanostatic test

Galvanostatic tests were performed for samples containing 40 and 50 vol.% aluminum oxide. Cycling was carried out at 110 °C in a symmetrical cell with lithium electrodes. The test sample was a disk of 2 cm² area with a thickness of 1 mm. The current density was 0.05 mA/cm². The results of galvanostatic cycling of the sample containing 50 vol.% Al_2O_3 are shown in Figure 6. It can be seen that the curves are symmetrical, indicating that the electrodes are identical. During the cycling, the voltage values were in the range of 1.5–1.6 V. At the same time, a slight increase in the potential during cycling was observed. The reason for this is most likely the formation of the SEI layer at the electrode/electrolyte interface.

The impedance hodograph of the cell and the equivalent circuit after galvanostatic tests are shown in Figure 7. The equivalent circuit includes 3 impedances connected in series: Z_1 – composite electrolyte resistance, Z_2 – charge transfer resistance and the electrode impedance represented by the constant phase element CPE_3.

$$Z_1 = [1/R_1 + Y_1^0(i\omega)^{n_1}]^{-1} \quad (4)$$

$$Z_2 = [1/R_2 + Y_2^0(i\omega)^{n_2}]^{-1} \quad (5)$$

$$CPE_3 = Y_3^0(i\omega)^{n_3} \quad (6)$$

The impedances (1) and (2) include the active resistances, R_1 and R_2, connected in parallel to the constant phase elements CPE_1 and CPE_2, respectively. Each CPE is defined by the terms Y_1^o, Y_2^o, and Y_3^o the exponents n_1, n_2, and n_3, respectively. The fitting of the theoretical dependence to the experimental data was carried out using the ZView program. The fitting curve is shown in Figure 7, and the parameters of the equivalent circuit are listed in Table 3.

Figure 8 shows the results of galvanostatic tests of a symmetric cell with a sample containing 40 vol.% Al_2O_3. The cycling was carried out at 110 °C in a symmetrical cell with lithium electrodes. The sample tested was a disk of 2 cm² area with a thickness of ~0.3 mm.

The current density was 0.05 mA/cm². It can be seen that qualitatively the results of cycling of this sample are similar to the results of galvanostatic tests of composite containing 50 vol% Al_2O_3. The results of galvanostatic cycling indicate that the samples under study have an appreciable contribution to lithium-ion conductivity.

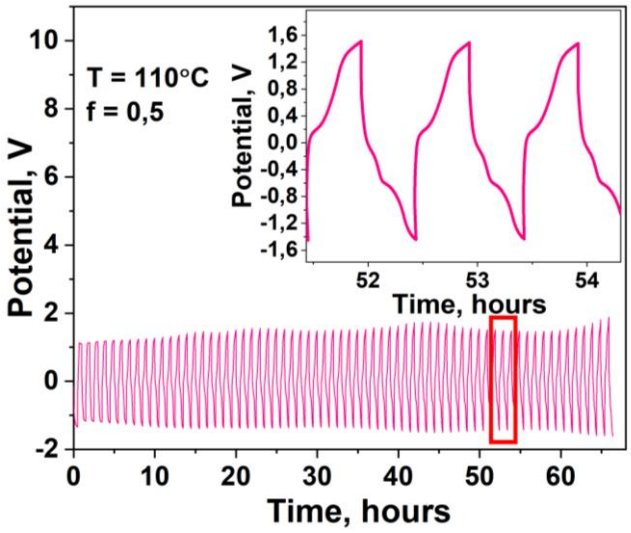

Figure 6 Galvanostatic cycling curve obtained for the cell Li/[0.82N_{13}pip]ClO_4-0.18$LiClO_4$-Al_2O_3/Li with the electrolyte containing $f(Al_2O_3)$ = 0.5.

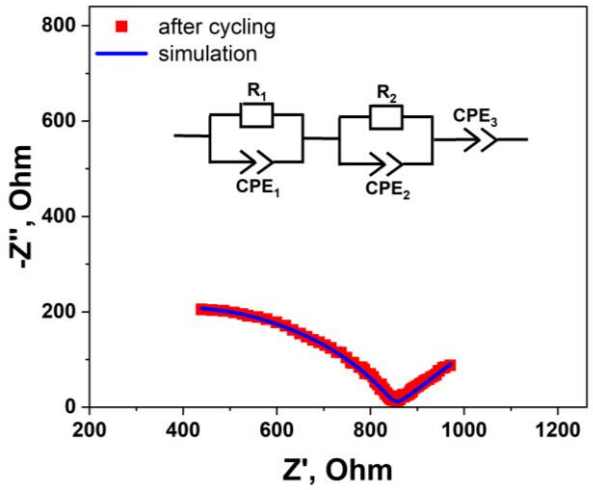

Figure 7 Nyquist curve obtained at 110 °C after galvanostatic cycling test for cell Li/[0.82N_{13}pip]ClO_4-0.18$LiClO_4$-Al_2O_3/Li containing $f(Al_2O_3)$ = 0.5.

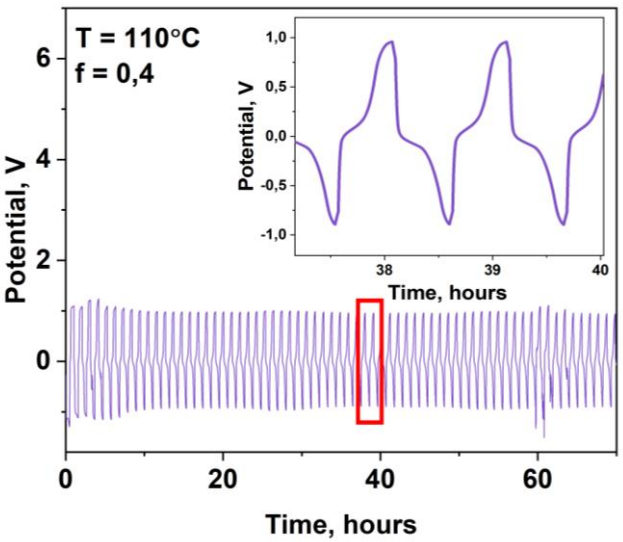

Figure 8 The galvanostatic cycling for 68 h for Li/[0.82N_{13}pip]ClO_4-0.18$LiClO_4$-Al_2O_3 /Li cell with volume fraction of Al_2O_3 f = 0.4.

 DOI:10.15826/chimtech.2024.11.3.04

Table 3 Equivalent circuit parameters obtained for the sample before and after galvanostatic cycling.

Parameter	Before cycling	After cycling
R_1	166±40	189±0,9
R_2	910±45	661±1
Y_1^o	$(2.7\pm0.7)\cdot10^{-7}$	$(1.1\pm0.1)\cdot10^{-6}$
n_1	0.73±0.05	0.61±0.01
Y_2^o	$(4.2\pm0.4)\cdot10^{-7}$	$(6.0\pm0.8)\cdot10^{-8}$
n_2	0.405±0.006	0,627±0.009
Y_3^o	$(2.3\pm0.1)\cdot10^{-4}$	$(4.15\pm0.05)\cdot10^{-3}$
n_3	0.64±0.01	0.407±0.007

It may be explained by the partial dissolution of lithium perchlorate in the amorphous phase of the organic salt.

3.5. Electrochemical stability

The electrochemical stability window of the composite concerning lithium was determined using the linear amperometry method in the voltage range of 0-5.5 V at a potential sweep rate of 1 mV/s in a cell where stainless steel (SS) was used as the working electrode (cathode) and lithium metal SS/[0.82N_{13}pip]ClO_4-$LiClO_4$-Al_2O_3/Li was used as the reference electrode (anode). As a test sample, a composite containing 50 vol% was taken. The obtained curve is shown in Figure 9. It can be seen that there is an increase in current up to 2 V after which the current value is near zero up to a voltage of ~3.7 V. From 3.7 V and up to ~4.4 V, an increase in current by ~2.5 mA is observed. Further, the current value does not change until ~4.8 V, after which the current starts to increase. A possible reason for such behavior is the formation of a passivation layer on the surface of the steel electrode in the voltage range of 3.7–4.4 V, which prevents further electrochemical decomposition up to 4.8 V. Thus, it can be concluded that this composite electrolyte remains stable up to 5 V.

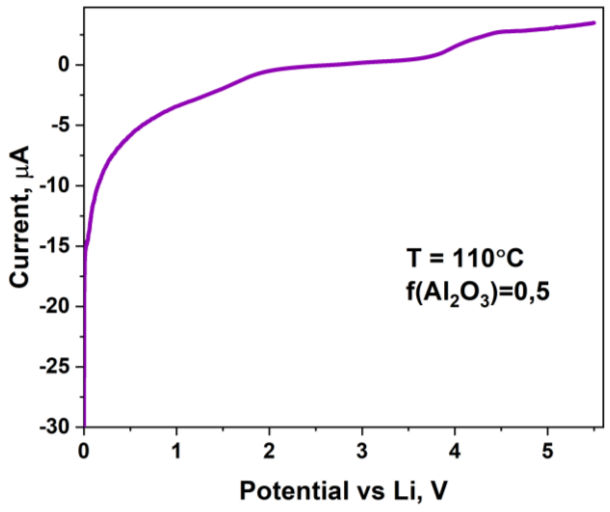

Figure 9 Linear voltammetry curve of Li/{[0.82N_{13}pip]ClO_4-0.18$LiClO_4$-Al_2O_3 /SS cell with volume fraction of Al_2O_3 f = 0.5.

4. Limitations

The mechanism of ion conduction in OIPC has not been fully understood at this time. There is ongoing debate in the literature about this topic. In this work, we propose a possible mechanism for ionic conductivity in a composite material based on OIPC. However, further research is needed to confirm this hypothesis. For example, techniques such as infrared (IR), nuclear magnetic resonance (NMR), and Raman spectroscopy could provide valuable insights into the physical and chemical processes that occur in composites.

5. Conclusions

The composites 0.82[N_{13}pip]ClO_4-0.18$LiClO_4$-Al_2O_3 obtained from eutectic mixture of the organic salt [N_{13}pip]ClO_4 and lithium perchlorate with the nanocrystalline additive of γ-alumina with the specific surface area of 200 m^2/g were synthesized, and their thermal, structural, transport and electrochemical properties were investigated. It was found that when a heterogeneous additive of aluminum oxide is added, the amorphization of the organic salt [N_{13}pip]ClO_4 takes place, and at the alumina volume fraction of f = 0.5 the salt completely transforms to the amorphous state.

At the same time, lithium perchlorate partially transfers from the bulk of the initial composite to the oxide surface. As a result, the composite becomes depleted in $LiClO_4$ as evidenced by the thermal analysis data. The conductivity of the composites increases with the alumina volume fraction. The maximum conductivity is achieved at the volume fraction of γ-Al_2O_3 f = 0.4–0.5. At such a concentration of the oxide, the conductivity exhibits non-Arrhenius behavior typical for amorphous conductors. According to galvanostatic cycling data, lithium ions give an appreciable contribution to the overall conductivity of the composites, and they can be used as solid electrolytes in lithium-ion batteries.

• Supplementary materials

No supplementary materials are available.

• Conflict of interest

The authors declare no conflict of interest.

• Acknowledgement

None.

• Funding

This work was report delivered at the X International Russia-Kazakhstan scientific-practical conference “Chemical Technologies of Functional Materials".

 DOI:10.15826/chimtech.2024.11.3.04

This work was supported by the Russian Science Foundation (grant no. 20-13-00302), https://www.rscf.ru/en.

• Author contributions

Conceptualization: N.U.
Data curation: D.K, A.U.
Formal Analysis: D.K., A.U.
Funding acquisition: Y.Y.Y., Z.Z.Z.
Investigation: D.K., A.U.
Methodology: A.U., N.U
Project administration: N.U.
Resources: N.U.
Supervision: N.U.
Validation: A.U., N.U.
Visualization: D.K.
Writing – original draft: D.K., A.U., N.U.

• Additional information

Author IDs:
Artem Ulihin, Scopus ID 15046088200;
Nikolai Uvarov, Scopus ID 7006949152.

Websites:
Institute of Solid State Chemistry and Mechanochemistry, http://www.solid.nsc.ru/en/institute/general/;
Novosibirsk State University, https://english.nsu.ru/.

References

1. Li Y, Huang W, Li Y, Pei A, Boyle DT, Cui Y. Correlating Structure and Function of Battery Interphases at Atomic Resolution Using Cryoelectron Microscopy. Joule. 2018;2(10):2167–2177. doi:10.1016/j.joule.2018.08.004
2. Matsumoto H, Sakaebe H, Tatsumi K. Preparation of Room Temperature Ionic Liquids Based on Aliphatic Onium Cations and Asymmetric Amide Anions and Their Electrochemical Properties as a Lithium Battery Electrolyte. J Power Sources. 2005;146(1):45–50. doi:10.1016/j.jpowsour.2005.03.103
3. MacFarlane DR, Forsyth M. Plastic Crystal Electrolyte Materials: New Perspectives on Solid State Ionics. Advanced Materials. 2001;13(12–13):957–966. doi:10.1002/1521-4095(200107)13:12/13<957::AID-ADMA957>3.0.CO;2-#.
4. Timmermans J. Plastic Crystals: A Historical Review. J Phys Chem Solids. 1961;18(1):1–8. doi:10.1016/0022-3697(61)90076-2
5. Thomas ML, Hatakeyama-Sato K, Nanbu S, Yoshizawa-Fujita M. Organic Ionic Plastic Crystals: Flexible Solid Electrolytes for Lithium Secondary Batteries. Energy Adv. 2023;2(6):748–764. doi:10.1039/D3YA00078H
6. Macfarlane DR, Kar M, Pringle J. Fundamentals of Ionic Liquids, From Chemistry to Applications. Wiley-VCH Verlag GmbH & Co. KGaA: Weinheim Germany, 2017. doi:10.1002/9783527340033
7. Kurtoğlu-Öztulum SF, Jalal A, Uzun A. Thermal Stability Limits of Imidazolium, Piperidinium, Pyridinium, and Pyrrolidinium Ionic Liquids Immobilized on Metal Oxides. Journal of Molecular Liquids. 2022;363:119804. doi:10.1016/j.molliq.2022.119804
8. Matuszek K, Piper SL, Brzęczek-Szafran A, Roy B, Saher S, Pringle JM, MacFarlane DR. Unexpected Energy Applications of Ionic Liquids. Adv Mater. 2024;36(23):2313023. doi:10.1002/adma.202313023
9. Brutti S, Simonetti E, De Francesco M, Sarra A, Paolone A, Palumbo O, Fantini S, Lin R, Falgayrat A, Choi H, Kuenzel M, Passerini S, Appetecchi GB. Ionic Liquid Electrolytes for High-Voltage, Lithium-Ion Batteries. J Power Sources. 2020;479:228791. doi:10.1016/j.jpowsour.2020.228791
10. Zhu H, MacFarlane DR, Pringle JM, Forsyth M. Organic Ionic Plastic Crystals as Solid-State Electrolytes. Trends Chem. 2019;1(1):126–140. doi:10.1016/j.trechm.2019.01.002
11. Park H, Park CB, Sung BJ. Simulation Studies on the Dynamic Heterogeneity of Organic Ionic Plastic Crystals. Bull Korean Chem Soc. 2023;44(9):736–749. doi:10.1002/bkcs.12715
12. Zhu H, Wang X, Vijayaraghava R, Zhou Y, MacFarlane DR, Forsyth M. Structure and Ion Dynamics in Imidazolium-Based Protic Organic Ionic Plastic Crystals. J Phys Chem Lett. 2018;9(14):3904–3909. doi:10.1021/acs.jpclett.8b01500
13. MacFarlane DR, Meakin P, Sun J, Amini N, Forsyth M. Pyrrolidinium Imides: A New Family of Molten Salts and Conductive Plastic Crystal Phases. J Phys Chem B. 1999;103(20):4164–4170. doi:10.1021/jp984145s
14. Jumaah FN, Mobarak NN, Hassan NH, Noor SAM, Nasir SNS, Ludin NA, Badri KH, Ahmad A, Ito ERD, Yoshizawa-Fujita M, Su'ait MS. Review of Non-Crystalline and Crystalline Quaternary Ammonium Ions: Classification, Structural and Thermal Insight into Tetraalkylammonium Ions. J Molecular Liquids. 2023;376:121378. doi:10.1016/j.molliq.2023.121378
15. Chen F, Jin L, de Leeuw SW, Pringle JM, Forsyth M. Atomistic Simulation of Structure and Dynamics of the Plastic Crystal Diethyl(Methyl)(Isobutyl)Phosphonium Hexafluorophosphate. J Chem Phys. 2013;138(24):244503. doi:10.1063/1.4811179
16. Biernacka K, Al-Masri D, Yunis R, Zhu H, Hollenkamp AF, Pringle JM. Development of New Solid-State Electrolytes Based on a Hexamethylguanidinium Plastic Crystal and Lithium Salts. Electrochimica Acta. 2020;357:136863. doi:10.1016/j.electacta.2020.136863
17. Ulihin A, Novozhilov D, Uvarov N. Solid Electrolytes in the N-Propyl-N-Methyl-Pyrrolidinium Tetrafluoroborate—Lithium Tetrafluoroborate System. Batteries. 2023;9(3). doi:10.3390/batteries9030167
18. Zhou Z-B, Matsumoto H. Lithium-Doped, Organic Ionic Plastic Crystal Electrolytes Exhibiting High Ambient-Temperature Conductivities. Electrochem Commun. 2007;9(5):1017–1022. doi:10.1016/j.elecom.2006.12.012
19. Seeber A, Forsyth M, M. Forsyth C, A. Forsyth S, Annat G, R. MacFarlane D. Conductivity, NMR and Crystallographic Study of N,N,N,N-Tetramethylammonium Dicyanamide Plastic Crystal Phases: An Archetypal Ambient Temperature Plastic Electrolyte Material. Phys Chem Chem Phys. 2003;5(12):2692–2698. doi:10.1039/B212743A
20. Uvarov NF. Composite Solid Electrolytes: Recent Advances and Design Strategies. J Solid State Electrochem. 2011;15(2):367–389. doi:10.1007/s10008-008-0739-4
21. Shekibi Y, Gray-Weale A, MacFarlane DR, Hill AJ, Forsyth M. Nanoparticle Enhanced Conductivity in Organic Ionic Plastic Crystals: Space Charge versus Strain Induced Defect Mechanism. J Phys Chem C. 2007;111(30):11463–11468. doi:10.1021/jp071631j
22. Ulikhin AS, Izmodenova AV, Uvarov NF. Effect of the Nature of a Heterogeneous Dopant on the Transport and Thermodynamic Properties of Composites Based on N-Methyl-n-Butylpiperidinium Tetrafluoroborate. Russ J Electrochem. 2024;60(1):67–72. doi:10.1134/S1023193524010130
23. Anion Effects on the Properties of OIPC/PVDF Composites. Materials Advances. 2021;2(5):1683–1694. doi:10.1039/doma00992j
24. Lennert A, Wagner K, Yunis R, Pringle JM, Guldi DM, Officer DL. Efficient and Stable Solid-State Dye-Sensitized Solar Cells by the Combination of Phosphonium Organic Ionic Plastic

Crystals with Silica. ACS Appl Mater Interfaces. 2018;10(38):32271–32280. doi:10.1021/acsami.8b12334
25. Ulikhin AS, Uvarov NF, Kovalenko KA, Fedin VP. Ionic Conductivity of Tetra-n-Butylammonium Tetrafluoroborate in the MIL-101(Cr) Metal-Organic Framework. Microporous and Mesoporous Mater. 2022;332:111710. doi:10.1016/j.micromeso.2022.111710
26. Maier J. Ionic Conduction in Space Charge Regions. Progress in Solid State Chem. 1995;23(3):171–263. doi:10.1016/0079-6786(95)00004-E
27. García Y, Porcarelli L, Zhu H, Forsyth M, Mecerreyes D, O'Dell LA. Probing Disorder and Dynamics in Composite Electrolytes of an Organic Ionic Plastic Crystal and Lithium Functionalised Acrylic Polymer Nanoparticles. J Magnetic Resonance Open. 2023;14–15:100095. doi:10.1016/j.jmro.2023.100095
28. Iranipour N, Gunzelmann DJ, Seeber A, Vongsvivut J, Doherty C, Ponzio F, O'Dell LA, Hollenkamp AF, Forsyth M, Howlett PC. Ionic Transport through a Composite Structure of N-Ethyl-N-Methylpyrrolidinium Tetrafluoroborate Organic Ionic Plastic Crystals Reinforced with Polymer Nanofibres. J Mater Chem A. 2015;3(11):6038–6052. doi:10.1039/C4TA07155G
29. Sakaebe H, Matsumoto H. N-Methyl-N-Propylpiperidinium Bis(Trifluoromethanesulfonyl)Imide (PP13-TFSI) - Novel Electrolyte Base for Li Battery. Electrochem Commun. 2003;5:594–598. doi:10.1016/S1388-2481(03)00137-1
30. Bushkova OV, Yaroslavtseva TV, Dobrovolskiy YuA. New Lithium Salts in Electrolytes for Lithium-Ion Batteries (Review). Russ J Electrochem. 2017; 53(7):677–669. doi:10.1134/S1023193517070035
31. Ulihin AS, Uvarov NF. Electrochemical Properties of Composition Solid Electrolytes LiClO4-MgO. Russ J Electrochem. 2009;45(6):707–710. doi:10.1134/S1023193509060135
32. Ulihin AS, Uvarov NF, Mateyshina YuG, Brezhneva LI, Matvienko AA. Composite Solid Electrolytes $LiClO_4$–Al_2O_3. Solid State Ionics. 2006;177(26):2787–2790. doi:10.1016/j.ssi.2006.03.018
33. Ulihin AS, Uvarov NF, Rabadanov KSh, Gafurov MM, Gerasimov KB. Thermal, Structural and Transport Properties of Composite Solid Electrolytes (1-x)(C4H9)4NBF4–xAl2O3. Solid State Ionics. 2022;378:115889. doi:10.1016/j.ssi.2022.115889
34. Mateyshina Y, Stebnitskii I, Shivtsov D, Ilyina E, Ulihin A, Bukhtiyarov A, Uvarov N. Hybrid Nanocomposite Solid Electrolytes (n-C4H9)4NBF4–MgO. Int J Molecular Sci. 2023;24(13). doi:10.3390/ijms241310949
35. Ulihin AS, Uvarov NF. Ionic Conductivity of Composite Solid Electrolytes $(C_4H_9)_4NBF_4$–Al_2O_3. Russian Journal of Electrochemistry. 2021;57(10):1015–1018. doi:10.1134/S1023193521080140
36. Wang X, Kerr R, Chen F, Goujon N, Pringle JM, Mecerreyes D, Forsyth M, Howlett PC. Toward High-Energy-Density Lithium Metal Batteries: Opportunities and Challenges for Solid Organic Electrolytes. Advanced Materials. 2020;32(18):1905219. doi:10.1002/adma.201905219
37. García Y, O'Dell LA. Understanding the Interfacial Region in Organic Ionic Plastic Crystal Composite Electrolyte Materials by Solid-State NMR. Current Opinion in Colloid & Interface Sci. 2022;61:101632. doi:10.1016/j.cocis.2022.101632
38. Zhu H. Structure and Ion Transport Properties of Organic Ionic Compounds Revealed by NMR. Magnetic Resonance Lett. 2024;4(2):100092. doi:10.1016/j.mrl.2023.11.004
39. Roggero A, Caussé N, Pébère N, Dantras E. VFT to Arrhenius Crossover at the Dynamic Glass Transition of an Epoxy Network as Revealed by Dielectric Experiments in Continuous Immersion. Polymer. 2022;241:124542. doi:10.1016/j.polymer.2022.124542
40. Liu GD, Wu JP, Dong HM, Zhang HQ. Nonlinear Modification of Vogel-Fulcher-Tamman (VFT) Model and Its Application in Enthalpy Relaxation of Glassy Polystyrene. J Non-Crystalline Solids. 2020;528:119761. doi:10.1016/j.jnoncrysol.2019.119761
41. Garca-Coln LS, del Castillo LF, Goldstein P. Theoretical Basis for the Vogel-Fulcher-Tammann Equation. Phys Rev B. 1989;40(10):7040–7044. doi:10.1103/PhysRevB.40.7040
42. Croce F, Appetecchi GB, Persi L, Scrosati B. Nanocomposite Polymer Electrolytes for Lithium Batteries. Nature. 1998;394(6692):456–458. doi:10.1038/28818
43. Duan T, Cheng H, Sun Q, Liu Y, Nie W, Chu Y, Xu Q, Lu X. Reinforcing Interfacial Compatibility of LLZTO/PVDF-HFP Composite Electrolytes by Chemical Interaction for Solid-State Lithium Metal Batteries. J Power Sources. 2024;589:233789. doi:10.1016/j.jpowsour.2023.233789
44. Rahman MYA, Ahmad A, Ismail LHC, Salleh MM. Fabrication and Characterization of a Solid Polymeric Electrolyte of PAN-TiO_2-$LiClO_4$. J Appl Polymer Sci. 2010;115(4):2144–2148. doi:10.1002/app.31299

 DOI:10.15826/chimtech.2024.11.3.04